

文章编号:1001-9014(2011)05-0385-04

Millimeter-wave balanced mixer based on a novel wide-band Schottky diode model

MOU Jin-Chao, LV Xin, YU Wei-Hua

(School of Information and Electronics, Beijing Institute of Technology, Beijing 100081, China)

Abstract: A Schottky diode model for the mixer's design is presented in this paper. According to the physical structure of the Schottky diode, a novel 3D electromagnetic (EM) model was built and analyzed by finite element method. A wide-band equivalent circuit up to 110 GHz was proposed taking the parasitic effects distributed in the diode into account. Based on the proposed equivalent circuit, a Ka-band balanced mixer was designed and optimized. The measured conversion loss is 7.5 dB to 10 dB from 32 GHz to 37 GHz, which agreed well with the simulated one.

Key words: Schottky diode; Ka band; balanced mixer; electromagnetic model; wide-band equivalent circuit

PACS: 84.40.Lj

基于新颖宽带肖特基二极管模型的毫米波平衡式混频器设计

牟进超, 吕昕, 于伟华

(北京理工大学信息与电子学院, 北京 100081)

摘要: 介绍了一个用于混频器设计的肖特基二极管模型. 根据二极管的物理结构, 建立了三维电磁模型, 并采用有限元法分析该模型. 根据二极管中分布的寄生效应, 建立了直到 110 GHz 的宽带等效电路. 基于该等效电路, 设计并优化了一个 Ka 频段的平衡式混频器. 在 32~37 GHz 频率范围内, 测试的变频损耗为 7.5~10 dB. 测试结果与仿真结果吻合地较好.

关键词: 肖特基二极管; Ka 波段; 平衡混频器; 电磁模型; 宽带等效电路

中图分类号: TN454 **文献标识码:** A

Introduction

Millimeter wave (MMW) and Sub-Millimeter wave (SMMW) imaging systems have many advantages, such as higher spatial resolution with the same antenna aperture compared to microwave imaging systems and the ability to work in low visibility conditions compared to infrared or optical imaging systems. For MMW and SMMW imaging systems, heterodyne receiver is a good choice, where the mixer is one of the most important components. It combines the input radio frequency (RF) signal and the local oscillating (LO) signal to produce an intermediate frequency (IF) signal, which

is a nonlinear process realized by nonlinear devices^[1].

Among the nonlinear devices in MMW and SMMW mixers, such as superconductor insulator superconductor (SIS) junctions^[2] and hot electron bolometers (HEBs)^[3], Schottky barrier diodes (SBDs) are fascinating due to the merits of low turn-on voltage and high response speed as well as easy fabrication and non-cryogenic condition requirement^[4]. Thus they are widely used in mixers and detectors^[4-8]. At MMW band, the performance of the Schottky diode can not be described by the classic equivalent circuit accurately because all the parasitic reactive elements are simply represented by a total shunt capacitance. One solution

Received date: 2010-12-03, **revised date:** 2011-01-01

收稿日期: 2010-12-03, **修回日期:** 2011-01-01

Foundation item: The National Basic Research Program of China (2010CB327505)

Biography: MOU Jin-Chao (1985-), male, Lianyungang, Jiangsu Province, China, Ph. D student. Research fields include millimeter-wave/Terahertz semiconductor devices and integrated circuits, E-mail: moujinchao@qq.com.

is to study the high frequency effects distributed in the Schottky diode and build an equivalent circuit taking all the parasitic elements into account. Instead of testing, a 3D EM model is analyzed by finite element method (FEM) and a wide-band equivalent circuit up to 110 GHz is built. Based on the proposed equivalent circuit, a Ka-band balanced mixer is designed and measured, the minimum conversion loss of which is 7.5 dB.

1 Schottky Diode and its Model

Fig. 1 illustrates the physical structure of the studied Schottky diode S0130 from *Beijing Institute of Technology*^[8]. The semi-insulating (S. I.) GaAs layer is used as the SBD's substrate. The epitaxial GaAs structure consists of a thick, heavily doped layer (n + GaAs) with a thin, lightly doped layer (n-GaAs) on its top. The anode formed on the n-GaAs layer leads to Schottky contact and the cathode pad formed on the n + GaAs layer results in ohmic contact. A finger is introduced to connect the anode and the anode pad, under which is an etched trench to reduce the parasitic capacitance between pads effectively. A silicon dioxide (SiO₂) layer on the top of the n-GaAs layer provides passivation and insulation. The detailed physical parameters of the Schottky diode are listed in Table. 1.

Table 1 Physical parameters of the studied SBD

表 1 所研究的肖特基二极管物理参数

Parameter	Value
n-GaAs Layer's Thickness/ μm	0.1
n-GaAs Layer's Doping density/ cm^{-3}	4E16
n + GaAs Layer's Thickness/ μm	3
n + GaAs Layer's Doping density/ cm^{-3}	3E18
S. I. GaAs Layer's Thickness/ μm	100
Trench Width/ μm	30
Anode Diameter/ μm	1.5

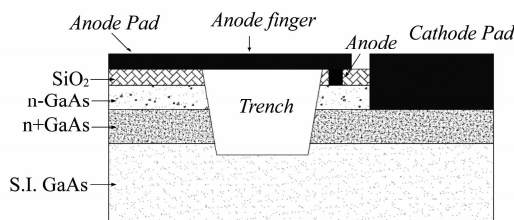


Fig. 1 Physical structure of the SBD S0130

图 1 SBDS0130 的物理结构

The current-voltage (I-V) characteristic of the Schottky diode satisfies the following relationship^[9]

$$I = I_s \left[\exp\left(\frac{q(V - IR_s)}{nkT}\right) - 1 \right], \quad (1)$$

where R_s is the series resistance; T is the physical temperature of the diode; n is the ideality factor and equals to 1 for an ideal diode; k is Boltzmann constant; I_s is the saturation current; q is the electric charge. According to the measured I-V curve plotted in Fig. 2, $R_s = 20 \Omega$, $n = 1.09$, $I_s = 9.8 \text{E} - 16 \text{ A}$, and the reverse break down voltage $V_{br} = 9.2 \text{ V} @ 20 \mu\text{A}$ are extracted.

The classic equivalent circuit of the Schottky diode is shown in Fig. 3. The desired mixing occurs in the nonlinear junction resistance $R_j(v)$. The series resistance R_s , junction capacitance $C_j(v)$ and shunt capacitance C_p are parasitic elements degrading the diode's performance. The series resistance R_s consists of metal loss as well as all resistances between the edge of the depletion region and the ohmic contact. The junction capacitance $C_j(v)$ is voltage dependent and consists of the capacitance due to the depletion region and the capacitance resulting from the fringing fields around the anode. The shunt capacitance C_p represents the total reactive parasitic effects of the diode excluding C_j , which is inherent in all planar diodes due to the distributed fringing fields and determined by the diode's geometry. The junction resistance R_j could be obtained by

$$R_j(v, i(v)) = \frac{nkT}{q(i(v) + I_s)}, \quad (2)$$

However, the classic equivalent circuit is too simple to reflect all the parasitic effects distributed in each

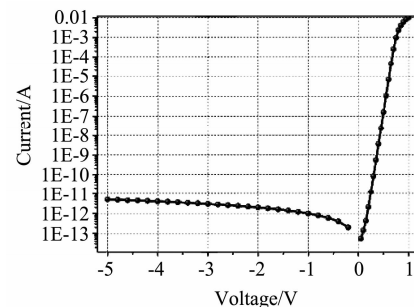


Fig. 2 Measured I-V curve of S0130

图 2 S0130 的测试伏安曲线

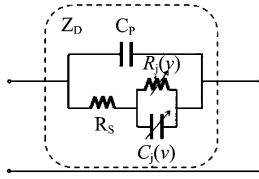


Fig. 3 Classic equivalent circuit of the Schottky diode
图3 肖特基二极管的经典等效电路

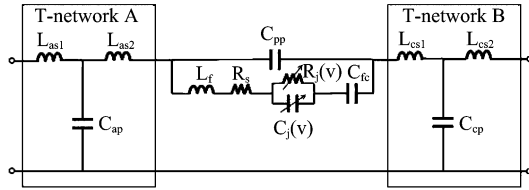


Fig. 4 Improved equivalent circuit of the Schottky diode
图4 肖特基二极管的改进等效电路

section and can not describe the phase accurately, especially in MMW and SMMW bands, which are critical for mixers' design. To solve this problem, an improved equivalent circuit shown in Fig. 4 is established according to the electromagnetic fields distributing in the SBD, taking all the parasitic effects into account. C_{pp} represents the fringing fields between the pads; T-network A and T-network B stem from the discontinuity of the anode pad and the cathode pad respectively; C_{fc} is the capacitance due to the fringing field of the finger and the finger is modeled as an inductor L_f .

To extract the equivalent elements, a lossless 3D EM model is built according to the diode's physical structure, as shown in Fig. 5. Some equivalent settings are introduced for 3D EM modeling, as summarized in Table. 2. The n-layer is divided into two sub-layers: a dielectric layer followed by a conducting layer. The thickness of the dielectric layer equals to the width of the depletion region in the n-GaAs layer, determined by^[9]

$$X_d = \begin{cases} \sqrt{\frac{2\epsilon_r\epsilon_0}{qN_{n-GaAs}} \left(V_{bi} - v - \frac{kT}{q} \right)} & X_d < t_{n-GaAs} \\ t_{n-GaAs} & X_d \geq t_{n-GaAs} \end{cases}, \quad (3)$$

where N_{n-GaAs} and t_{n-GaAs} are the doping density and thickness of the n-GaAs layer respectively. The 3D model under the zero-bias condition is calculated using finite element method and the S-parameters are given in Fig. 6. All the reactance components including C_j

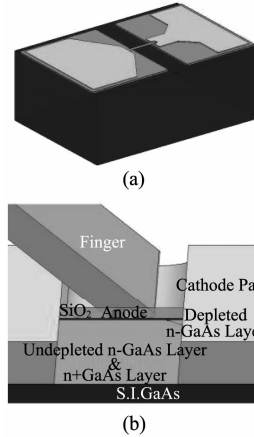


Fig. 5 3D EM model of the SBD S0130
图5 SBD0130 的三维电磁模型

can be extracted from the EM analyzed results, and the extracted reactance parameters are listed in Table. 3. The S-parameters of the equivalent circuit excluding R_j and R_s are also plotted in Fig. 6, which agree well with the EM simulated ones up to 110 GHz.

Table 2 Equivalent settings of the SBD's EM model
表2 SBD 电磁模型等效设置

Region	Material used in HFSS
depleted n-GaAs layer	GaAs with a thickness of X_d , $\epsilon_r = 12.9$
n + GaAs layer & undepleted n-GaAs layer	perfect conductor
pads and finger	perfect conductor
S. I. GaAs substrate	GaAs, $\epsilon_r = 12.9$
SiO ₂ layer	Silicon Dioxide, $\epsilon_r = 4$

In order to show the validity of the proposed model, the studied SBD with its test structures is fabricated using GaAs process. A Cascade's probe station together with a HP 8510C network analyzer (up to 40 GHz)

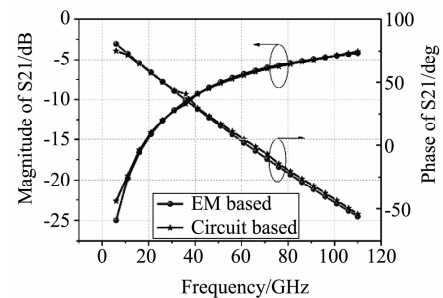


Fig. 6 S-parameters of the SBD S0130 from EM based model and its equivalent circuit excluding R_j and R_s
图6 SBDS0130 的电磁模型 S 参数以及不包含 R_j 和 R_s 的等效电路 S 参数

is used for S-parameter measurement. The thru-reflect-line (TRL) de-embedding technique^[10] is adopted to obtain the de-embedded S-parameters of the Schottky diode. Fig. 7 shows the comparison of the measured and circuit-based S-parameters, both the amplitude and the phase of the measured S-parameters agree well with the simulated ones.

Table 3 Extracted parasitic reactance elements
表 3 提取的寄生感性元件

C_{pp}/fF	C_{ap}/fF	L_{as1}/pH	L_{as2}/pH	L_j/nH
11.47	25.76	17.48	24.26	2
C_{cp}/fF	L_{cs1}/pH	L_{cs2}/pH	C_{jc}/fF	C_j/fF
29.9	62	27.17	3.5	1.3

2 Design and Realization of the Mixer

Fig. 8 shows the topology of the designed balanced mixer^[11], consisting of a rat-race coupler, two band pass filters (BPFs), a low pass filter (LPF) and two Schottky diodes. The substrate used is Rogers 5880 with the thickness of 0.254 mm and the relative dielectric constant of 2.2.

The rat-race coupler consists of four $\lambda/4$ arms and a $\lambda/2$ section, where λ is the wavelength on the microstrip line at 35 GHz. The simulated results are illustrated in Fig. 9.

The RF BPF and LO BPF are used to prevent IF leakage into the RF port and LO port respectively, both of which use five-order parallel coupled lines. The center frequency of the two BPFs is 35 GHz with the bandwidth of 10 GHz. The simulated results of the two BPFs are shown in Fig. 10. The function of the LPF at the IF port is to provide isolation between the IF port and the RF port as well as the LO port. A five-order

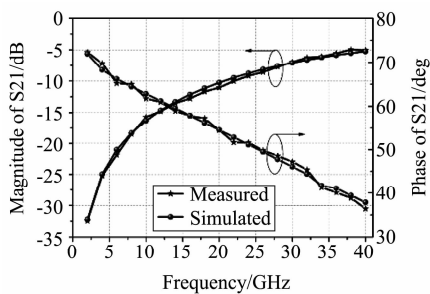


Fig. 7 Comparison between the measured S-parameters and the circuit-based ones
图 7 测量的 S 参数和等效电路对应的 S 参数

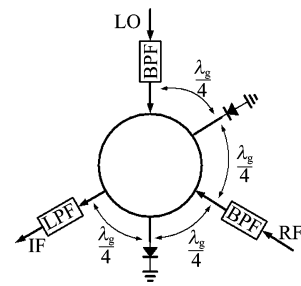


Fig. 8 Topology of the 180° balanced mixer
图 8 180°平衡式混频器拓扑图

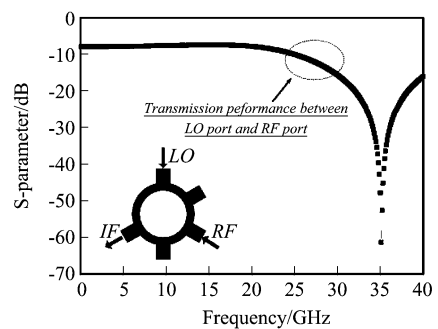


Fig. 9 Simulated S-parameters of the rat-race coupler
图 9 环形电桥的仿真 S 参数

hammer head LPF^[6] is used for good rejection at Ka band, as shown in Fig. 11.

The total mixer is analyzed using harmonic balance simulator in Agilent's ADS, where the Schottky diode model consists of an intrinsic diode and parasitic elements as shown in Fig. 12. By tuning the length of the microstrip lines between diodes and the rat-race coupler, the conversion loss L_c could be optimized, which is defined as

$$L_c = 10 \log_{10} \left(\frac{P_{RF}^{avail}}{P_{IF}} \right) (\text{dB}) \quad , \quad (1)$$

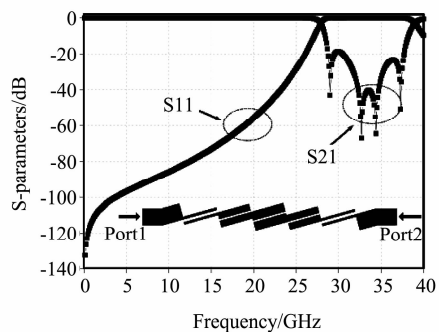


Fig. 10 Simulated S-parameters of the BPFs
图 10 带通滤波器的仿真 S 参数

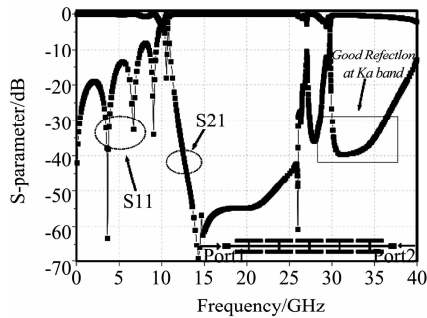


Fig. 11 Simulated S-parameters of the LPF
图 11 低通滤波器的仿真 S 参数

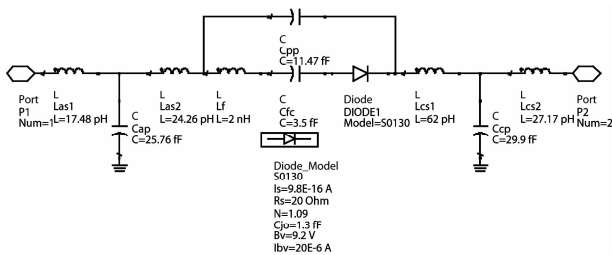


Fig. 12 Diode model in ADS
图 12 二极管的 ADS 模型

P_{RF}^{avail} is the available RF input power and P_{IF} is the IF output power.

The optimized mixer was fabricated using lithography technology. An E8363B vector network analyzer is used for S-parameter measurement and the measured results are shown in Fig. 13. Two E8257D signal generators and one E4447A spectrum analyzer are used for conversion loss measurement. Under the LO input power of 10 dBm, the conversion loss is 7.5 dB to 10 dB from 32 GHz to 37 GHz with IF fixed at 1 GHz, as shown in Fig. 14. The measured results show good agreement with the simulated ones, implying the validity of the proposed diode model.

3 Conclusion

The key device in a mixer is the Schottky diode for creating new frequency components, whose accurate model is crucial for mixer design. According to the SBD's physical structure, a 3D EM model was built and a wide-band equivalent circuit up to 110 GHz was proposed. Based on the equivalent circuit, a Ka-band balanced mixer was designed and fabricated. The measured conversion loss is less than 10 dB over the frequency range from 32 GHz to 37 GHz, which agrees

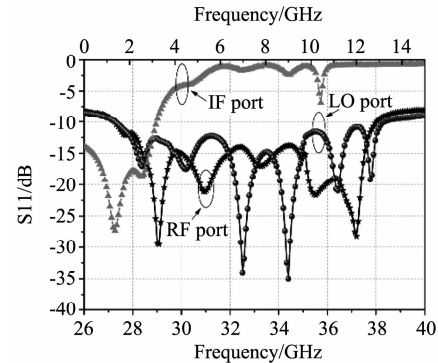


Fig. 13 Measured S11 of RF port, LO port, IF port, respectively

图 13 RF 端口、LO 端口以及 IF 端口的测试 S11

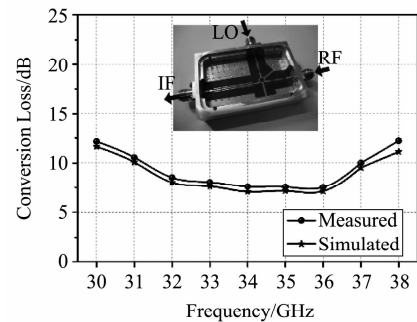


Fig. 14 Conversion loss of the balanced mixer and its photograph

图 14 平衡式混频器的变频损耗以及其照片

well with the simulated one, showing the validity of the proposed model.

REFERENCES

- [1] HÜBERS Heinz-Wilhelm. Terahertz Heterodyne Receivers [J]. *IEEE Journal of Selected Topics in Quantum Electronics*, 2008, **14**(2): 378 - 391.
- [2] ZHANG Wen, SHAN Wen-Lei, SHI Sheng-Cai. Investigation of Embedding Impedance Characteristics for a 660 GHz Waveguide SIS Mixer [J]. *J. Infrared Millim. Waves* (张文, 单文磊, 史生才. 660 GHz 频段波导型 SIS 混频器嵌入阻抗的特性研究. *红外与毫米波学报*), 2002, **21**(6): 465 - 468.
- [3] GAO J R, HAJENIUS M, YANG J J, *et al.* Terahertz Super-conducting Hot Electron Bolometer Heterodyne Receivers [J]. *IEEE Transactions on Applied Super-conductivity*, 2007, **17**(2): 252 - 258.
- [4] OXLEY H. Terry. 50 Years Development of the Microwave Mixer for Heterodyne Reception. *IEEE Transactions on Microwave Theory and Techniques*, 2002, **50**(3): 867 - 876.
- [5] ZHOU Mi, XU Jun, LUO Shen-du, *et al.* Ka-band Fourth Harmonic Mixer with 1-D EBG Structure [J]. *J. Infrared Millim. Waves* (周密, 徐军, 罗慎独, 等. 一种使用一维电磁带隙结构 Ka 频段四次谐波混频器. *红外与毫米波学报*), 2006, **25**(2): 147 - 149.

(下转 450 页)

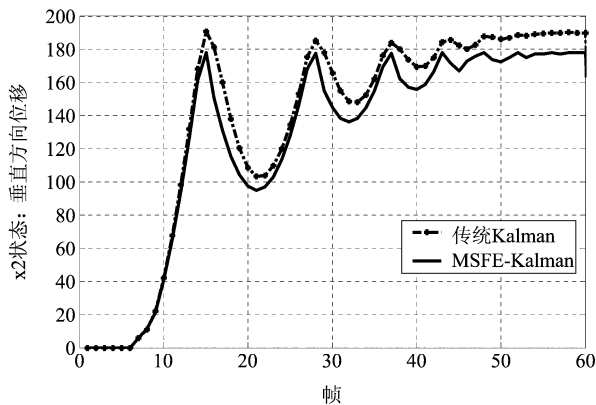


图5 Kalman 和 MSFE-Kalman 垂直方向位置状态对比
Fig. 5 The vertical position's state contrast between Kalman and MSFE-Kalman

为了进一步说明本文所描述滤波的优点,现将 MSFE-Kalman 算法和传统 Kalman 算法在对小球的垂直方向位置状态估计进行对比,如图 5. 在目标状态估计时,由于引入 MSFE 图像配准作为滤波的约束条件,所以得到观测信号相比传统算法精确度要高,而且获取时间也较短. 从图中对比可看出,实线的峰值较虚线的峰值超前,说明 MSFE-Kalman 滤波算法时效性强;另外实线的峰值几乎都稳定在同一个峰值上(本次实验稳定值为 177.833 左右),说明 MSFE-Kalman 滤波算法的收敛性很高.

4 结语

本文针对波动性较大的运动目标跟踪问题,提出了一种基于多尺度特征点提取(MSFE)的 Kalman 滤波的跟踪算法. 该算法将 MSFE 特征点配准作为约束条件引入 Kalman 滤波方程,以前帧图像中目标所匹配出的后续帧图像目标区域上的特征点为中心,建立目标小范围搜索区域,避免对整幅图像进行遍历的传统算法,同时所匹配出的特征点具有目标位置标定作用,为当前时刻状态后验估计提供稳定

且精确的观测值和观测残差,从而提高 Kalman 滤波的鲁棒性和时效性. 实验证明,基于 MSFE 的 Kalman 滤波算法在跟踪波动性较大的运动目标,其状态各个分量都能得到快速且有效地收敛.

REFERENCES

- [1] Bakowki A, Jones G A. Video surveillance tracking using colour region adjacency graphs[J]. *IEEE Conference Publication*. 1999,2(465):794-798.
- [2] Wixson L. Detecting salient motion by accumulating directionally-consistent flow[J]. *IEEE Transactions of Pattern Analysis and Machine Intelligence*. 2000,22(8):774-780.
- [3] XIN Yun-Hong, YANG Wan-Hai. Pseudo-linear kalman filter with application to the passive tracking of multi-stations IRSTS[J]. *J. Infrared Millim. Waves*(辛云宏,杨万海. 基于伪线性卡尔曼滤波的多站 IRST 系统跟踪技术. *红外与毫米波学报*),2005,24(5):374-377.
- [4] A Shahbahrami, B Juurlink, S Vassiliadis. Accelerating color space conversion using Extended subwords and the matrix register file[C]. *Eighth IEEE International Symposium on Multimedia*,2006:37-46.
- [5] David G. Lowe. Object recognition from Local scale-invariant features[J]. *International Conference on Computer Vision, Corfu, September,1999*,3(1):1150-1157.
- [6] David G. Lowe. Distinctive image features from scale-invariant keypoints[J]. *International Journal of Computer Vision*. 2004. 60(2):91-110.
- [7] Kong Jun, Tang Xin-Yi, Jiang Min. Object location technique for moving target based on multi-scale feature extraction[J]. *J. Infrared Millim. Waves*(孔军,汤心溢,蒋敏. 基于多尺度特征提取的运动目标定位研究. *红外与毫米波学报*),2011,30(1):21-26.
- [8] WANG Hong-Bing, PENG Zhen-Ming, LIU Jie, et al. Feature points detection and tracking based on SIFT combining with KLT method[J]. *Proc. SPIE*. 2009(7506):75062N1-10.
- [9] R E Kalman, A new approach to linear filtering and prediction problem[J]. *Trans on ASME. Journal of Basic Engineering*,1960,82(1):35-45.
- [10] Kalman R E, Bucy R S. New methods and results in linear filtering and prediction theory[J]. *Trans on ASME, Journal of Basic Engineering*,1961,83:95-108.
- [11] Meyn S P, Lyndon J B, Model reference adaptive control of time varying and stochastic systems[J]. *IEEE Trans on Auto Control*,1993,38(2):1739-1753.

(上接 389 页)

- [6] YU Wei-Hua, MOU Jin-Chao, LI Xiang, et al. Design of a W band Subharmonically pumped Mixer Based on a hybrid Schottky Diode Model[C]. *2009 International Conference on Microwave Technology and Computational Electromagnetics*,2009:207-210.
- [7] YANG Zi-Qiang, YANG Tao, LIU Yu. Design of Ka-band monolithic image rejection mixer[J]. *International Journal of Infrared and Millimeter Waves*,2007,28(3):237-241.
- [8] MOU Jin-Chao, YUAN Yong, YU Wei-Hua, et al. Design and Fabrication of planar GaAs Schottky Barrier Diodes for Submillimeter-wave Applications[C]. *International Confer-*

ence on Microwave and Millimeterwave Technology, 2010: 1746-1749.

- [9] RHODERICK E H. Metal-semiconductor contacts[C]. *IEE Proceedings-Communications*,1982,129(1):1-14.
- [10] ENGEN G F, HOER C A. Thru-Reflect-Line: An Improved Technique for Calibrating the Dual Six-Port Automatic Network Analyzer[J]. *IEEE Transactions on Microwave Theory and Techniques*,1979,27(12):987-993.
- [11] WANG Chuang, GU Jianzhong, SUN Xiaowei. Low cost compacted Ka-band rat-race mixer[C]. *Asia-Pacific Conference Proceedings*,2005.